

Article

Hybrid Effect of Basalt and Polyacrylonitrile Fibers on Physico-Mechanical Properties of Tailing Mortar

Jianbo Xu ¹, Zhijie Pi ^{2,*}, Shibing Huang ^{2,3,*} , Yan Zhang Liu ^{2,3}, Ziwen Chen ² and Yongqi Shen ²¹ China First Metallurgical Group Co., Ltd., Wuhan 430080, China; xujb@cfmcc.com² School of Resources and Environmental Engineering, Wuhan University of Science and Technology, Wuhan 430081, China; liuyanzhang@wust.edu.cn (Y.L.); 13571901339@163.com (Z.C.); shenyongqi1999@163.com (Y.S.)³ Hubei Key Laboratory for Efficient Utilization and Agglomeration of Metallurgic Mineral Resources, Wuhan 430081, China

* Correspondence: pizhijie1534010242@163.com (Z.P.); huangshibing@wust.edu.cn (S.H.)

Abstract: In this study, 50% iron ore tailings (IOTs) were used to prepare the cemented mortar at low economic costs and with great environmental benefits. Basalt fiber (BF) and polyacrylonitrile fiber (PANF) were added to the tailing mortar to improve the comprehensive performance of tailing mortars, including BF (0~0.5%), PANF (0~0.05%) and the combination of them. The results show that the addition of BF and PANF can significantly improve the ultrasonic velocity, uniaxial compressive strength (UCS), split-tensile strength (STS), flexural strength (FS) and toughness of the tailing mortar. A novel finding is that the enhancement of hybrid fibers is much better than single fiber, and the best hybrid fiber combination is B0.25P0.05 (0.25 wt% BF and 0.05 wt% PANF), because this combination not only causes the most considerable increase in strength but also possesses great cost-effectiveness. Compared to the B0P0 group without fibers, the maximum increments of B0.25P0.05 in UCS, STS and FS are 45.74%, 52.33% and 15.65%, respectively. It is evidenced that the improvement in STS is the largest because the fibers have good cracking resistance and bridging effect in the tailing mortar. The scanning electron microscope (SEM) further confirms that too many hybrid fibers will agglomerate and produce more voids, which is harmful to the development of the internal structure. Beyond B0.25P0.05, the hydration products are also reduced due to the decrease in nucleation sites, observed by combining X-ray diffraction (XRD) tests. Therefore, it is suggested that the hybrid fibers containing 0.25% BF and 0.05% PANF should be used in this tailing mortar.

Keywords: sulfur-containing tailings; basalt fiber; polyacrylonitrile fiber; physico-mechanical properties; fiber-reinforced tailing mortar



Citation: Xu, J.; Pi, Z.; Huang, S.; Liu, Y.; Chen, Z.; Shen, Y. Hybrid Effect of Basalt and Polyacrylonitrile Fibers on Physico-Mechanical Properties of Tailing Mortar. *Buildings* **2024**, *14*, 639. <https://doi.org/10.3390/buildings14030639>

Academic Editor: Elena Ferretti

Received: 24 December 2023

Revised: 16 February 2024

Accepted: 19 February 2024

Published: 29 February 2024



Copyright: © 2024 by the authors. Licensee MDPI, Basel, Switzerland. This article is an open access article distributed under the terms and conditions of the Creative Commons Attribution (CC BY) license (<https://creativecommons.org/licenses/by/4.0/>).

1. Introduction

Concrete and mortar are the most widely used construction materials in civil engineering, and approximately 25 billion tons are consumed per year [1]. River sand accounts for about 25% of the concrete. In China, the annual consumption of river sand exceeds 20 billion tons. In addition, the overexploitation or even depletion of river sand has occurred in some areas. This phenomenon has also caused a series of serious ecological destruction and geological disasters [2]. Therefore, it is urgent to seek fine aggregates that can replace river sand, which is also required for the sustainable production of concrete, environmental protection and ecological balance. Iron ore tailings (IOTs) are the waste residue after separating iron ore concentrate [3]. Currently, the storage of IOTs in China has exceeded 5 billion tons and is growing rapidly at an annual rate of more than 300 million tons. Due to the low utilization ratio, a large amount of IOTs can only be piled up in tailing ponds, which not only encroach on the land and pollute the surrounding environment, but also require a large amount of maintenance funds [4–6]. To protect the environment and increase the economic benefits, the secondary use of IOTs in the construction industry has

attracted the attention of many scholars [7,8]. Andrews et al. [9] found that the compressive strength and splitting tensile strength of concrete were greatly improved with a 25% IOT substitution. Zhang et al. [10] and Zhao et al. [11] also observed that the maximum compressive strength of concrete could be derived with a 40% replacement of river sand by IOTs. Huang et al. [12] found that the strength of mortar by adding 50% IOTs did not decline compared with the mortar with complete standard sand. Therefore, IOTs can be used as fine aggregate in cemented materials.

However, concrete with a high IOT replacement ratio may also suffer from a low mechanical strength, poor cracking resistance and weak ductility [13,14]. Therefore, fibers are introduced to further improve the mechanical strength and overcome the brittle failure problem [15–18]. In general, the utilization of single fiber only enhances the properties of cemented materials in a certain aspect. For example, High et al. [19] and Zhang et al. [20] reported that basalt fiber (BF) significantly enhanced the tensile strength and flexural strength, but the improvement in compressive strength was insignificant. In addition, Chinchillas et al. [21] claimed that polyacrylonitrile fiber (PANF) could improve the flexural strength much more than the compressive strength. Conversely, the synergistic effect of hybrid fibers may contribute to improving the overall performance through a multi-scale reinforcement mechanism [22–24]. Walton et al. [25] found that the addition of hybrid inorganic and organic fibers in concrete could increase its impact and tensile properties. Wang et al. [26] illustrated that the compressive, tensile and flexural strengths of concrete were greatly improved by the incorporation of hybrid basalt and polypropylene fibers. Currently, the recommended hybrid fiber is the combination of rigid and flexible fibers. Rigid fibers with a high elastic modulus improve the strength of cemented materials, while flexible fibers with a low elastic modulus effectively inhibit the generation and development of cracks [27]. Besides, to reduce the production cost and achieve a high performance of cemented materials, the hybrid fibers with a good price and high quality are needed urgently. Basalt fibers (BFs) are made from basalt ores, which have the advantages of a low production cost, high tensile strength, high modulus of elasticity and good corrosion resistance [28–30]. In addition, BF has better compatibility with cemented materials due to their similar chemical composition [31,32]. Therefore, BF has been widely used in the engineering construction industry [33,34]. Polyacrylonitrile fiber (PANF) is a kind of green, flexible and low-cost material with excellent tensile and crack resistance [35,36]. PANF is a reinforcing material for concrete because it has a positive effect on the improvement in tensile strength, durability and toughness [37,38]. Zeng et al. [39] reported that BF and PANF fiber-reinforced concrete had better mechanical properties and toughness than single fiber-reinforced concrete. However, previous studies have mainly focused on a single kind of fiber, and the combination effect of hybrid BF and PANF fibers in mortars is not fully understood, particularly in tailing mortars. In addition, the best hybrid fiber content in the mortar is significantly influenced by the aggregate, such as tailings. It is essential to investigate the best combination and optimal additive content of hybrid BF and PANF fibers by considering the overall physico-mechanical performance and production costs of the tailing mortar.

The main objective of this study is to investigate the effect of BF, PANF and hybrid fibers on the physico-mechanical properties of fresh and hardened tailing mortars. The specific aims are as follows: (1) to investigate the effect of single and hybrid fibers on the common physico-mechanical properties of tailing mortar; (2) to evaluate the synergetic effect and cost of fiber-reinforced tailing mortar; (3) to interpret the reinforced mechanism of BF and PANF on the tailing mortar by using SEM and XRD tests; (4) to quantify the most economical and high-performance additive content of hybrid fiber for the tailing mortar with 50% replacement of standard sands.

2. Materials and Methods

2.1. Materials

2.1.1. Cement

The cement is P·O 42.5 produced by Huaxin Cement Co., Ltd. (Ezhou, China), according to Chinese standard GB 175-2007 [40]. The properties and composition are shown in Table 1.

Table 1. Main properties and composition of the cement.

Properties	Value	Element	Cement/wt%
Specific surface area (m ² /kg)	351	CaO	57.18
Soundness	qualified	SiO ₂	21.97
Initial setting time/min	230	Al ₂ O ₃	6.55
Final setting time/min	300	SO ₃	4.68
3-day compressive strength/Mpa	28.6	Fe ₂ O ₃	2.89
3-day flexural strength/Mpa	5.4	MgO	2.14
Loss on ignition/%	3.73	K ₂ O	0.958
		P ₂ O ₅	0.509

2.1.2. Aggregates

The aggregates utilized in this study were standard sand (SS) and IOTs. The SS was produced by Xiamen ISO Standard Sand Co., Ltd. (Xiamen, China) (GB/T 17671-2021 [41]) and the main chemical composition was quartz (>98%). The IOTs were selected from a tailing reservoir in Ezhou City, Hubei Province. The chemical composition of the IOTs was measured by XRF and XRD (Table 2, Figure 1), which showed that the main minerals were quartz, sulfide, calcite, etc. Obviously, they are a type of high-sulfur tailings. After drying at 105 °C for 24 h, the fineness modulus of SS and IOTs was determined at 2.38 and 1.54 by the sieving tests, respectively (Figure 2). According to the GB/T 14684-2022 [42], the IOT is too fine to meet the construction requirements. Therefore, further experiments were conducted by mixing IOTs with SS to effectively utilize the IOTs. Earlier works have demonstrated the viability of mixed sand that contains 50% SS and 50% IOTs [12]. The gradation curve of mixed sand was produced through the sieving test, as shown in Figure 2. The fineness modulus of mixed sand is 1.96. Table 3 displays the physical properties of SS, IOTs and mixed sand. The particle gradation and void fraction of mixed sand were improved.

Table 2. Chemical properties of IOTs.

Elements	SiO ₂ (%)	CaO (%)	SO ₃ (%)	Fe ₂ O ₃ (%)	Al ₂ O ₃ (%)	MgO (%)	K ₂ O (%)	Na ₂ O (%)
IOTs/wt%	24.70	19.10	15.06	11.56	6.88	3.86	2.96	1.63

Table 3. Physical properties of SS, IOTs and mixed sand.

Type	Loose Bulk Density (kg/m ³)	Compact Bulk Density (kg/m ³)	Apparent Density (kg/m ³)	Loose Void Ratio (%)	Compacted Void Ratio (%)
SS	1654.47	1735.17	2656.07	37.7	34.7
IOTs	1737.57	1963.13	3104.05	44.0	36.8
Mix sand	1689.84	1857.20	2874.96	41.2	35.4

2.1.3. Fibers

Table 4 lists the morphological and physical characteristics of fibers. Because the size of themortar specimen and aggregates is small, the suitable lengths of BF and PANF are 6 mm and 12 mm, respectively. Figures 3 and 4 depict the macromorphology and micromorphology of fiber filaments. The BF is a rigid fiber with smooth surface, while PANF is a flexible fiber with a relatively rough surface. Before mixing, a hair dryer was used to disperse the fibers in a closed container to avoid fiber aggregation.

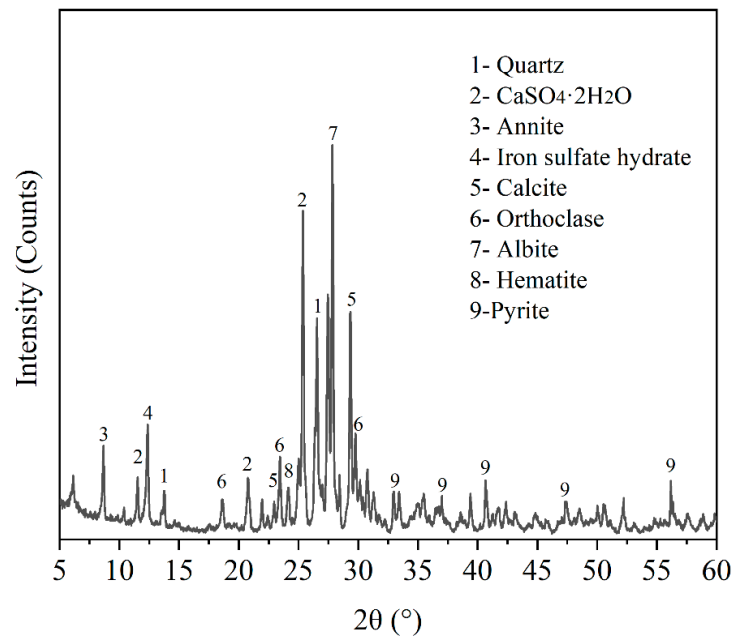


Figure 1. XRD pattern of IOTs.

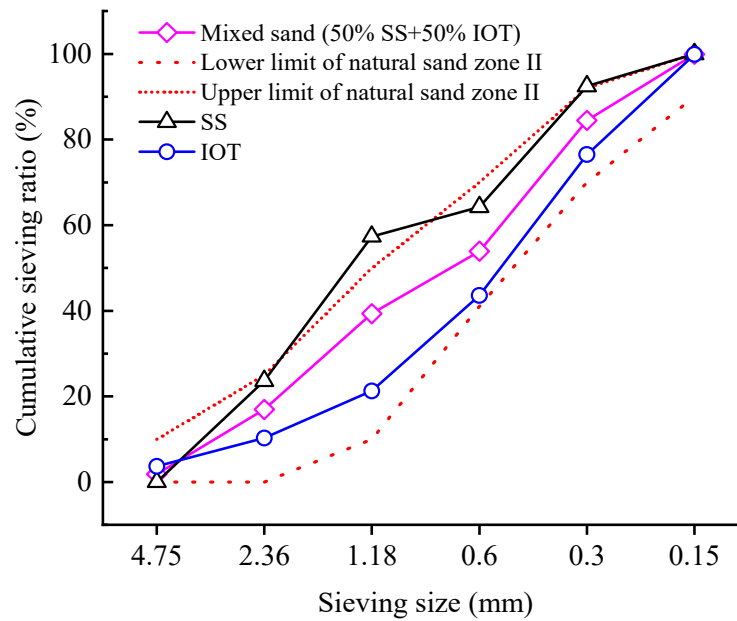


Figure 2. Gradation curve of the SS, IOTs and mixed sand.

Table 4. Physical properties of fibers.

Fiber Type	Length /mm	Diameter / μm	Density/(g/cm^3)	Tensile Strength/MPa	Elastic Modulus/GPa	Elongation/%
PANF	12	13	1.18	530	7.2	22
BF	6	17	2.7	1650	63	2.8

2.1.4. Water and Super-Plasticizer

Water was taken from local tap water in Wuhan city. Polycarboxylic super-plasticizer (SP) was used to improve the fluidity and strength of the mortar.

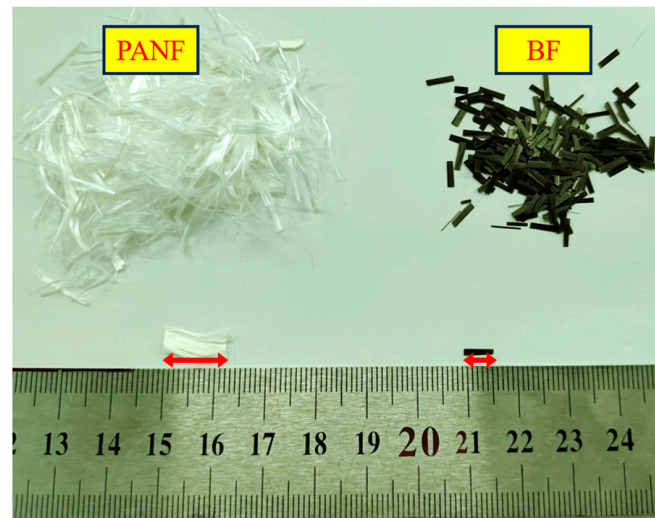


Figure 3. Macromorphology of fiber filaments.

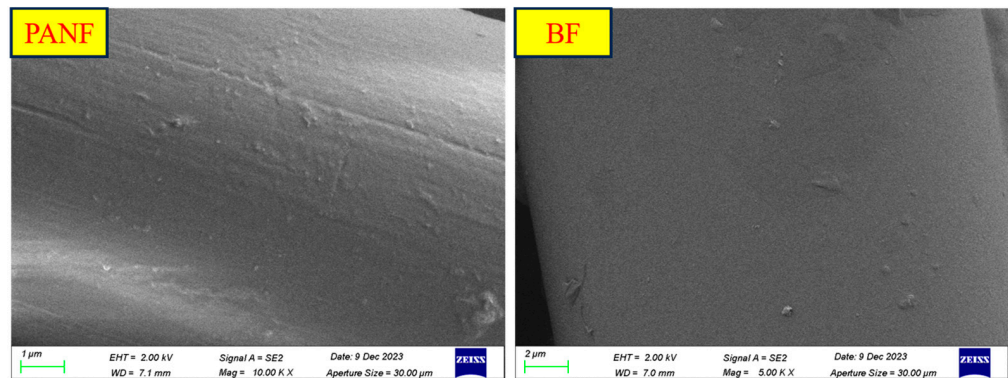


Figure 4. Micromorphology of fiber filaments.

2.2. Specimen Preparation

To explore the effect of hybrid fibers by combining BF and PANF on the tailing mortar, 12 different mixture proportions were designed in this study. The agglomeration of excessive fibers significantly influences the fluidity of mortar; therefore, the BF content was 0.25% and 0.5%, and the PANF content was set as 0.01%, 0.03% and 0.05%, respectively. The cement/SS/IOTs/water/SP = 400:600:600:168:2. Therefore, all of the tailing mortar with 12 different contents of fibers can be divided into 5 kinds of single fiber-reinforced mortar, 6 kinds of hybrid fiber-reinforced mortar and 1 kind of mortar without fibers.

The mixing process was carried out according to Chinese standard JTG 3420-2020 [43]. First, the dry SS and IOTs were mixed in a mixer for 1 min. Second, cement and fibers were added in sequence and mixed for 1 min and 2 min, respectively. Third, the water was added with the simultaneous addition of SP to stir for 5 min. The stirring process included slow stirring at 135 r/min for 2 min followed by fast stirring at 270 r/min for another 3 min. Therefore, the fresh hybrid fiber-reinforced tailing mortar (HRTM) could be derived. The fluidity and density tests were conducted first on the fresh mortar. Then, it was poured into the molds with dimensions of $70.7 \times 70.7 \times 70.7 \text{ mm}^3$ and $40 \times 40 \times 160 \text{ mm}^3$. To remove the entrapped air from the matrix, an external shaking table was used to vibrate matrix for 10 s. All specimens were demolded after being cured for 24 h ($20 \text{ }^\circ\text{C}$, 90 RH%). Thereafter, the specimens were cured in a standard curing box for 28 d ($20 \pm 2 \text{ }^\circ\text{C}$, $\geq 95 \text{ RH}\%$). The detailed mixing and curing process is shown in Figure 5. The specimens of $70.7 \times 70.7 \times 70.7 \text{ mm}^3$ were used for the uniaxial compression test and splitting tensile test, and the $40 \times 40 \times 160 \text{ mm}^3$ specimens were used to conduct the flexural test and ultrasonic wave velocity test.

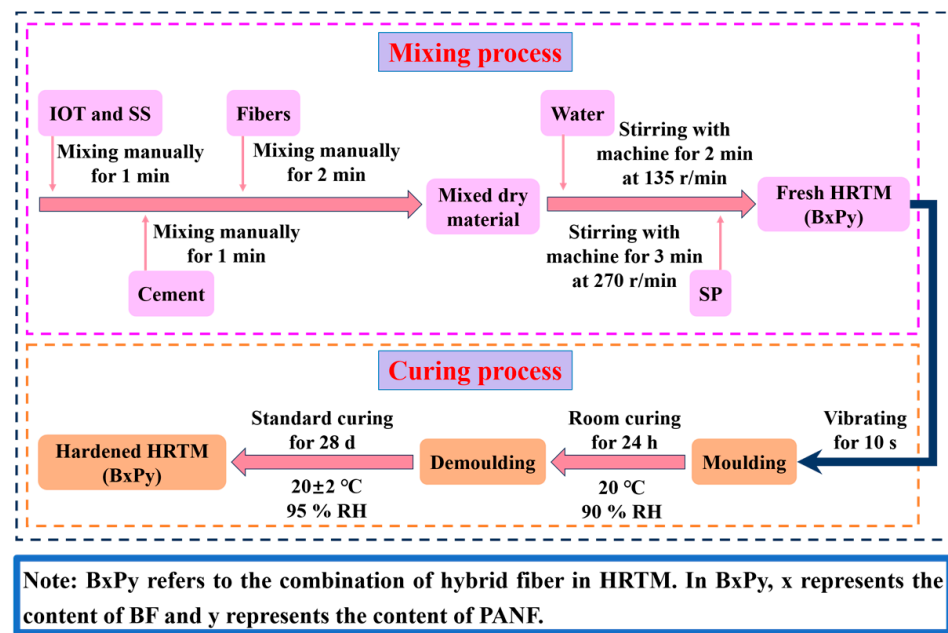


Figure 5. The detailed mixing and curing process.

2.3. Testing Procedure

2.3.1. Fluidity Test

Fluidity and density tests were performed according to Chinese standard JTG 3420-2020 [43]. The consistency was used to quantify the fluidity of fresh mortar. Mortar consistency is the penetration depth of the standard cone into the mortar by self-weight after 10 s. Therefore, a mortar consistometer (Tongli, SZ-145) was used to test the consistency in order to investigate the influence of fiber content on the fluidity of fresh mortar. In addition, the densities of hardened tailing mortars after curing for 28 d were also tested.

2.3.2. Ultrasonic Velocity Test

The primary wave (P-wave) and secondary wave (S-wave) velocities of specimens against curing ages were measured by a non-metallic acoustic wave detector (RSM-SY6C). The velocities were calculated as follows.

$$V = \frac{S}{t} \times 10^6 \quad (1)$$

V is the wave velocity (m/s), S is the interval between transducers (m), and t is the time (μ s).

According to ASTM C597-09 (2009) [44], the dynamic modulus of elasticity was calculated as follows:

$$E_d = \frac{(1 + \mu)(1 - 2\mu) \times v_p^2 \times \rho}{(1 - \mu)} \times 10^{-9} \quad (2)$$

E_d is the modulus of dynamic elasticity (GPa), v_p is the P-wave velocity (m/s), ρ is density (kg/m^3) and μ is the Poisson ratio.

The Poisson ratio can be expressed as follows:

$$\mu = \frac{v_p^2 - 2v_s^2}{2v_p^2 - 2v_s^2} \quad (3)$$

v_s is the S-wave velocity (m/s).

2.3.3. Mechanical Test

The uniaxial compressive strength (UCS), split tensile strength (STS) and flexural strength (FS) of tailing mortar were tested referring to the Chinese standard JTG 3420-2020. The mechanical strengths were measured by using a hydraulic servo-controlled mechanical machine. To reduce errors caused by the molding process and test conditions, three specimens were used for the same condition. The loading rates were 1.5 kN/s, 0.08 Mpa/s and 50 N/s for the uniaxial compressive, split tensile and flexural strengths, respectively. The mechanical test process is displayed in Figure 6.



Figure 6. Schematic diagram of the mechanical tests.

2.3.4. Porosity Test

The damaged specimens ($40 \times 40 \times 160 \text{ mm}^3$) were cut into three smaller specimens with dimensions of $40 \times 40 \times 40 \text{ mm}^3$ for the porosity test. These specimens were first dried at $105 \text{ }^\circ\text{C}$ for 24 h to reach a constant weight m_d . Thereafter, the completely dried specimens were placed in a vacuum saturation device (Huida, ZK-270; Cangzhou, China) for 48 h at -0.1 MPa . The saturated mass was recorded as m_s . Therefore, the porosity can be calculated as follows:

$$n = \frac{m_s - m_d}{\rho_w V_s} \times 100\% \quad (4)$$

n is the porosity (%), m_s is the mass of the saturated specimen (g), m_d is the mass of the completely dried specimen (g), ρ_w is the density of water (1 g/cm^3) and V_s is the volume of the specimen (cm^3).

2.3.5. Microstructural Analysis

The crushed specimens from mechanical tests were selected for microstructure analysis by using scanning electron microscopy (SEM) and XRD. These crushed specimens were first kept in ethanol to prevent the hydration process and preserve their original pore characteristics. Thereafter, they were dried in an oven at $65 \text{ }^\circ\text{C}$ until they reached a constant weight. The drying temperature was controlled at $65 \text{ }^\circ\text{C}$ to avoid the destruction of hydration products [45].

To observe the micromorphology of hydration products and the interaction between the fibers and the matrix, several specimens with different fiber contents were selected for SEM (ZEISS GeminiSEM 300) tests. These test pieces were smaller than $10 \text{ mm} \times 10 \text{ mm} \times 20 \text{ mm}$. When carrying out tests, the pieces were coated with a gold film to improve the conduction and hence the image quality. The acceleration voltage was 3 kV and the scale bar of the images was $10 \text{ }\mu\text{m}$.

To analyze the crystalline phase in hydration products, the XRD tests were carried out by a diffractometer (Bruker D8 Advance, copper target). The 2-theta range was from 5° to 60° at a scanning rate of $2^\circ/\text{min}$. Small pieces were cut from the core of the crushed specimens and ground into powders for XRD tests.

3. Results and Discussion

3.1. Fluidity and Density

Table 5 shows the fluidity of mortar specimens against fiber types and contents. The fluidity of tailing mortar displays a decreasing trend compared to the control group. The minimum fluidity occurs in the B0.50P0.05 group, decreasing by 33.11%. The addition of BF and PANF increases the friction of tailings to promote the interlocking effect [46–48]. In addition, fibers also absorb some water to reduce the water film thickness (WFT) on the mortar matrix and thus further reduce the fluidity of tailing mortar [49]. For single BF, it does not have a significant effect on fluidity. This may be attributed to the relatively smooth surface and short length of BF, which cannot easily form the network structure. Conversely, due to the rougher surface, larger length (12 mm) and greater water absorption capacity, the adverse effect of PANF on the fluidity is greater than BF. In addition, the addition of hybrid fibers further significantly reduces the fluidity of the mortar compared to the single fibers. The fiber combination (BF: 6 mm; PANF: 12 mm) more easily forms a network structure inside the mortar specimens. Additionally, with increasing fiber content, the specific surface area of the mortar increases and more cement paste is wrapped around the fiber surface [50].

Table 5. The fluidity and density results of the mortar specimens.

Notation	Consistency /cm	Decrement/%	Fresh Density /(kg/m^3)	Increment/%	Hardened Density /(kg/m^3)	Increment/%
BOP0	10.33	0.00	1873.1	0.00	2016.2	0.00
BOP0.01	8.9	13.84	1904.5	1.68	2046.3	1.49
BOP0.03	8.23	20.33	1934.8	3.29	2055.8	1.96
BOP0.05	8.07	21.88	1950.2	4.12	2064.6	2.40
B0.25P0	10.28	0.48	1884.2	0.59	2032.5	0.81
B0.50P0	10.2	1.26	1893.3	1.08	2044.1	1.38
B0.25P0.01	8.62	16.55	1977.1	5.55	2087.4	3.53
B0.25P0.03	7.98	22.75	2048.1	9.34	2099.2	4.12
B0.25P0.05	7.13	30.98	2075.8	10.82	2148.5	6.56
B0.50P0.01	8.52	17.52	2013.2	7.48	2105.2	4.41
B0.50P0.03	7.48	27.59	2054.8	9.70	2140.8	6.18
B0.50P0.05	6.91	33.11	1970.5	5.20	2081.2	3.22

The densities of the fresh and hardened mortar specimens are also presented in Table 5. The fresh and hardened densities show a similar variation trend. When one type of fiber is added, the density increases. The BF improves the density of the tailing mortar because it has a greater density than the matrix [51]. However, it can be observed that when 0.25 wt% or 0.5 wt% BF is added, the fresh densities of B0.25P0 and B0.5P0 do not show any significant increase. First, there is an intrinsic link between the consistency of the mortar and the fresh density. The fluidity of B0.25P0 and B0.5P0 is very close (10.28 cm, 10.20 cm), which will not cause any difference in the fresh density. In addition, the basalt fiber contents in mortar are in smaller quantities and thus contribute less to the fresh density. Li et al. [52] also found that the wet pack densities of mortar with 0–0.5% BF raise slightly with increasing BF contents. PANF is longer and more likely to form a network structure to compact the tailing mortar and further increase the density. In addition, the flexible PANF has a smaller diameter and better dispersion in the tailing mortar, which can easily fill into and pass through the pores between the fine aggregates to increase the density (Figure 7). This finding is consistent with previous research [53]. Therefore, when the hybrid fibers are added to the tailing mortar, the density increases significantly. However, excessive added fibers can agglomerate together and introduce some air into the mortar, resulting in an increase in the porosity and a reduction in the density [54].

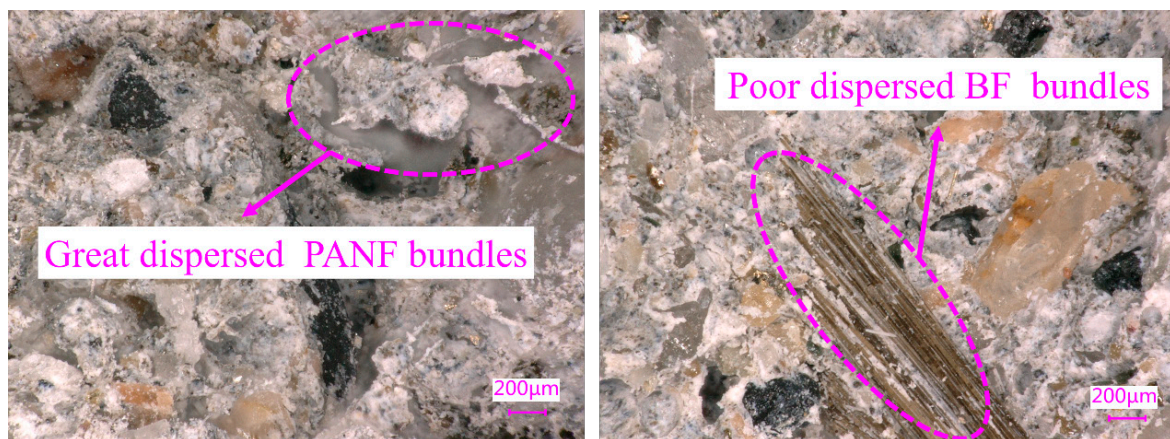


Figure 7. The dispersion of single PANF and BF bundles in the mortar specimens.

3.2. Porosity

Figure 8 displays the variation in porosity against the BF and PANF contents. It is evident that the addition of fibers significantly decreases the porosity compared with the control mixture. The fibers have a bridging effect that fills the pores and prevents the growth of cracks, thus reducing the porosity. When single BF fibers are added at 0.25% and 0.5%, the porosity decreases by 2.23% and 4.70%, respectively. Additionally, by increasing single PANF to 0.01%, 0.03% and 0.05%, the porosity decreases by 0.73%, 2.05% and 2.85%, respectively. This shows that the improvement in relatively low fiber content is not significant due to the weak bridging effect. Compared to the single type of fibers, hybrid fibers cause a greater improvement in porosity (Figure 8). Additionally, the B0.25P0.05 group of specimens have minimum porosity at 18.54%, which is 25.55% lower than the control group. With increasing fiber contents, the bridging effect is gradually developed to form the dense three-dimensional network structure. However, when the hybrid fiber content exceeds the critical value, poor dispersion occurs and more pores are produced, which causes an increase in the porosity [55]. The porosity of the B0.50P0.05 group is only 5.10% lower than the control mix.

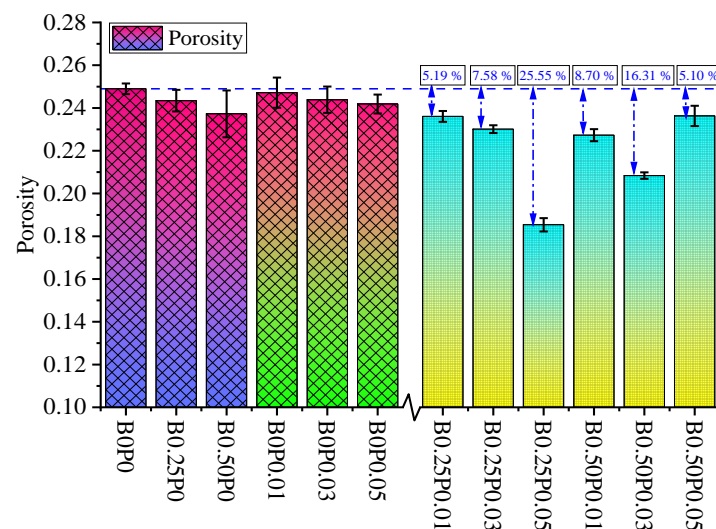


Figure 8. The porosity of the mortar specimens.

3.3. Ultrasonic Velocity

Figures 9–11 show the variation in P-wave velocity, S-wave velocity and the dynamic modulus of elasticity against the curing age and fiber contents. When increasing the curing age, they have the same growth trend due to the continuous hydration reaction

of the cement matrix and production of hydration products [56]. The addition of BF and PANF significantly increases the ultrasonic velocity compared to the control mix. When single BF or PANF are added, the ultrasonic velocity increases with increasing fiber content. In terms of hybrid fibers, when the BF content is 0.25%, they increase quickly with increasing PANF content. However, at a 0.50% BF content, they first increase but then decrease with the increasing content of PANF. For hybrid fiber specimens, the B0.25P0.05 group and B0.50P0.05 group possess the maximum and minimum ultrasonic velocities, respectively. For example, the P-wave velocity, S-wave velocity and dynamic elastic modulus of the B0.25P0.05 group at 28 d are 7.39%, 5.75% and 20.52% higher than the B0P0 group. Additionally, the P-wave velocity, S-wave velocity and dynamic elastic modulus of the B0.50P0.05 group at 28 d are only 2.87%, 2.52% and 8.68% higher than the B0P0 group, respectively. Overall, the increment in the ultrasonic velocity by adding hybrid fibers is better than a single fiber. The correlation between the ultrasonic velocity and porosity is also significant (Figure 12). In addition, although the tailing mortar and the concrete are different kinds of cemented materials, they have very similar physico-mechanical properties. Due to the lack of sufficient research on the tailing mortar, a similar relationship between the ultrasonic velocity and porosity for concrete can be also found in Benaicha [56] and Ridengaoqier [57], which further verifies the reliability of the present results.

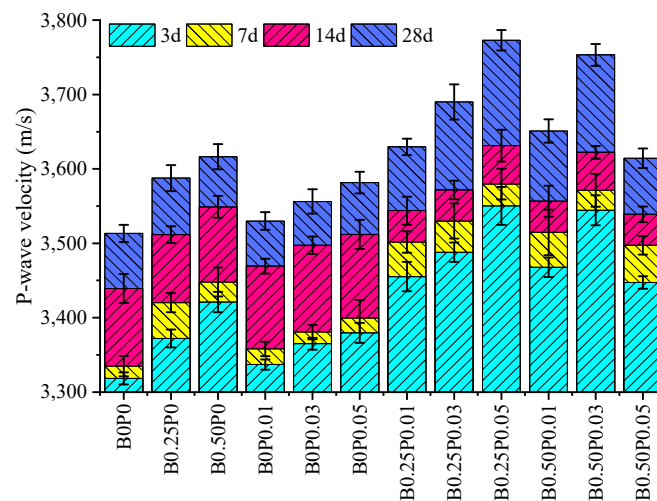


Figure 9. The P-wave velocity against the added content of fibers.

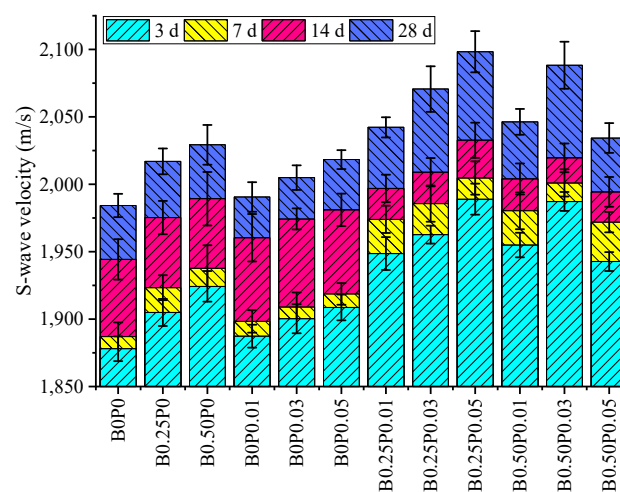


Figure 10. The S-wave velocity against the added content of fibers.

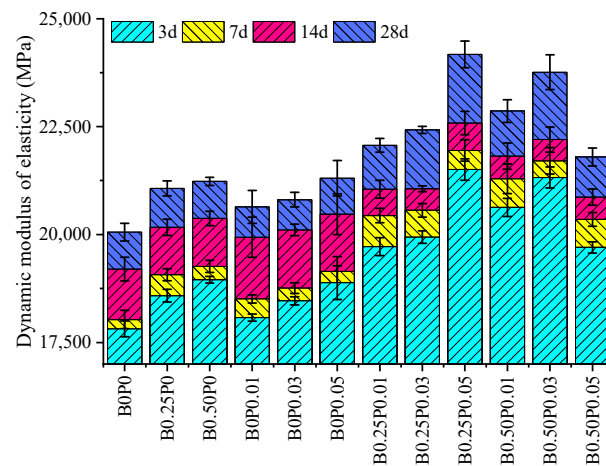


Figure 11. The dynamic modulus of elasticity against the added content of fibers.

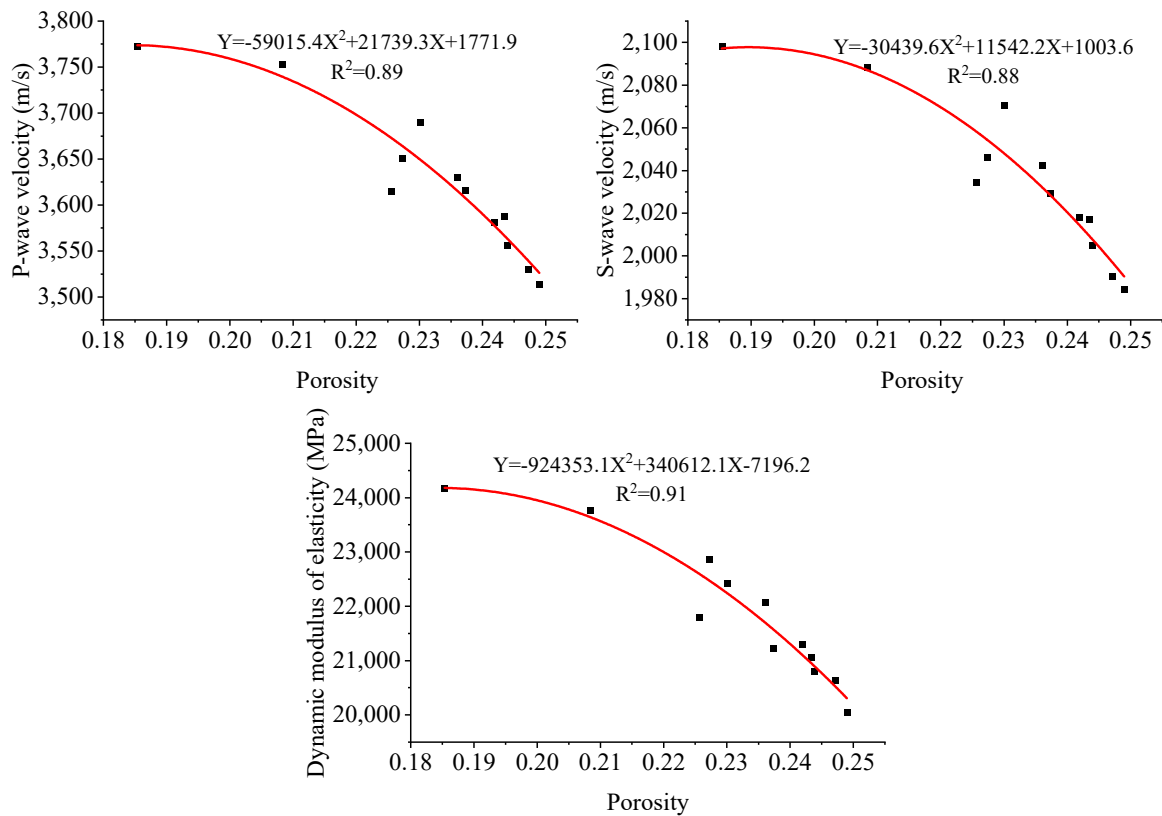


Figure 12. The relationship between the ultrasonic velocity (28 d) and porosity.

3.4. Mechanical Strength

3.4.1. Uniaxial Compressive Strength (UCS)

The UCS of specimens containing different fiber contents are presented in Figure 13. The increment in UCS is given in Table 6. It is observed that the maximum UCS value (30.08 MPa) occurs in the B0.25P0.05 group, which is 45.74% higher than in the control group. During the compression process, the fibers can bear a lot of loads and the friction between the fibers and the matrix prevents the formation and expansion of cracks [58,59]. For a single addition of BF or PANF, the UCS increases with increasing fiber content. Compared to the B0P0 group, the UCS of B0.25P0 and B0.50P0 increases by 13.78% and 17.38%, respectively. However, for mortar specimens with PANF, the increase in UCS is not significant, only 2.91%, 8.45% and 10.07%, respectively, because the bridging effect and

cracking resistance effect are poor for a low PANF content. In addition, it is a consensus that the bridging effect of flexible fibers is more effective in tensile conditions rather than compressive conditions [60,61]. Obviously, the contribution of hybrid fibers to the increase in UCS is better than of a single fiber. According to previous research [62–64], flexible PANF (12 mm) in the mortar more easily forms a network structure and prevents the formation and propagation of microcracks, while rigid BF (6 mm) has a better stiffness to bear more shear loads and restrict the deformation of hardened specimens. Therefore, hybrid fibers can complement each other in terms of elastic modulus and they can form a better three-dimensional network structure. In addition, hybrid fibers with different lengths can restrict different crack widths under loading [65]. Therefore, the combination of hybrid fibers is better to enhance the UCS. However, the excessive hybrid fibers agglomerate together and absorb more water, reducing the fluidity and producing more pores inside the mortar [66]. Therefore, the UCS reduces if too many hybrid fibers are added; for example, B0.50P0.05 has a much lower UCS than B0.25P0.05. It can be concluded that the best hybrid fiber combination is B0.25P0.05 for this tailing mortar.

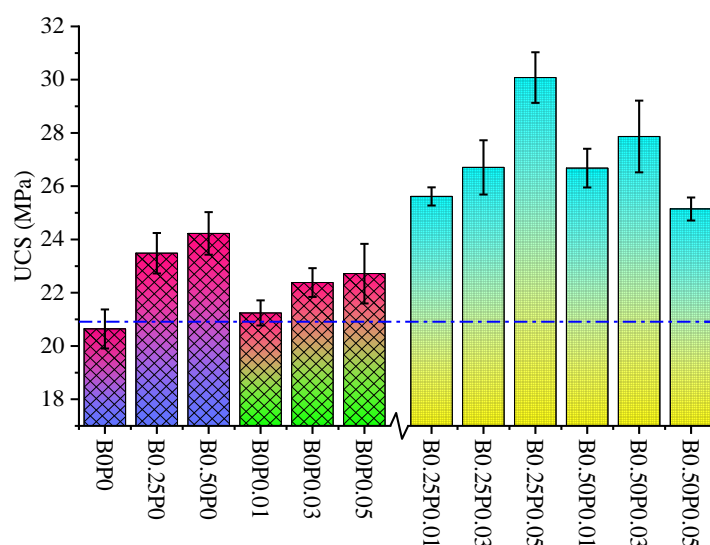


Figure 13. The UCS against incorporated fiber contents.

Table 6. The mechanical strength increments of mortar specimens with fibers.

Number	Increment		
	UCS	STS	FS
B0P0	0	0	0
B0.25P0	13.78%	9.04%	1.58%
B0.50P0	17.38%	10.99%	5.19%
B0P0.01	2.91%	3.85%	1.05%
B0P0.03	8.45%	10.29%	4.69%
B0P0.05	10.07%	14.49%	7.93%
B0.25P0.01	24.10%	28.55%	6.11%
B0.25P0.03	29.39%	33.41%	9.36%
B0.25P0.05	45.74%	52.33%	15.65%
B0.50P0.01	29.26%	28.84%	6.71%
B0.50P0.03	35.02%	36.25%	10.03%
B0.50P0.05	21.83%	22.67%	0.50%

The typical failure modes of the specimens after compressive tests are shown in Figure 14. The yellow line indicates the direction of crack propagation. The specimens with a low fiber content exhibit obvious shear failure characteristics and brittle failure mode. At its peak strength, the specimen ruptures suddenly and the main crack penetrates the specimen. With increasing fiber content, a three-dimensional network structure is

formed which fills the internal pores and changes the propagation direction of microcracks. In addition, the main crack width decreases and many secondary cracks are observed, displaying better integrity and toughness [63]. However, excessive hybrid fiber has induced more defects, and a wider main crack occurs in the specimens during loading process. Therefore, the addition of hybrid fibers significantly improves the toughness of specimens. The failure mode also confirms that the best fiber combination is B0.25P0.05.

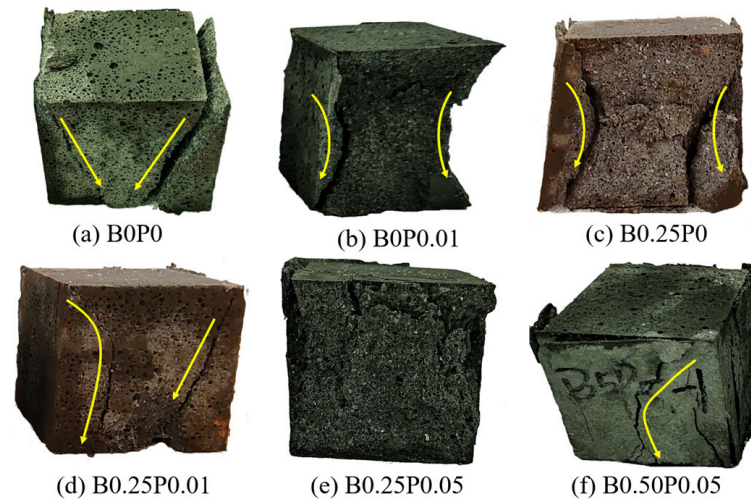


Figure 14. Typical failure mode of mortar specimens after compressive tests.

3.4.2. Split Tensile Strength (STS)

STS against fiber content is presented in Figure 15. It is evident that fibers significantly improve the STS of specimens. The increment ratio is from 3.85% to 52.33% (Table 6). The contribution of PANF to the STS is larger than that of the BF, which is opposite to the UCS. The longer flexible PANF more easily forms a network structure and possesses a better bridging effect; therefore, the bridging effect of PANF is more effective under tensile conditions. The detailed reinforced mechanism of PANF and BF can be explained as follows. PANF has a great dispersion of fiber bundles and distributes uniformly, which can delay the formation and propagation of microcracks during the hardening process. Under loading, the rigid BF can bear loads and limit the propagation of cracks. Figure 16 shows the microscopic distribution of PANF and BF in the mortar. This further confirms that PANF mainly inhibits the propagation of microcracks. PANF is prone to rupture in the crack area, and only when the PANF content increases to a certain amount are the cracking resistance and bridging effect obvious. Therefore, the hybrid fiber-reinforced specimens have the combination advantages of PANF and BF, and thus exhibit a better STS than the single fiber-reinforced specimens. For example, compared to the B0P0 group, the increment ratio of the B0.25P0.05 group is up to 52.33%. The greater improvement due to hybrid fibers was also found by Niu [62] and Sadrinejad [64]. The negative effect of excessive fibers on the STS are the same as on the UCS. The specimens in the B0.25P0.05 group have the maximum STS.

Figure 17 displays the typical failure modes of specimens after flexural tests. The cracks completely penetrate the B0P0 and B0P0.01 specimens after failure. With the increase in fiber content, the width and length of the crack decrease, and the propagation direction is significantly influenced by the fibers. Therefore, this implies that the fibers effectively prevent the development of cracks. However, the poor dispersion of too many hybrid fibers in B0.25P0.05 specimens cause the production of many pores, thus resulting in a wider and longer main crack.

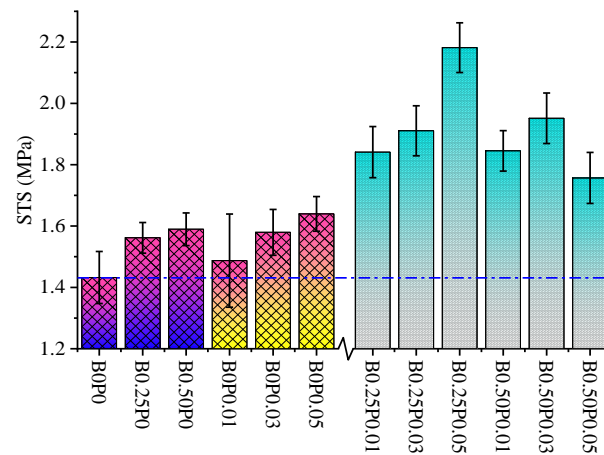


Figure 15. The STS against fiber content.

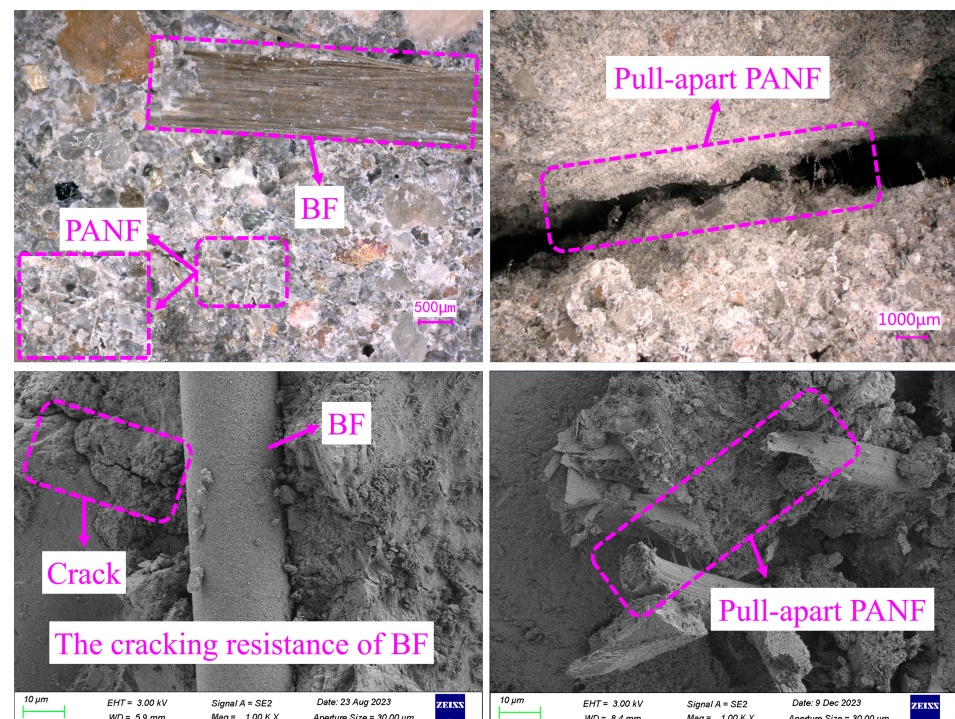


Figure 16. The distribution of PANF and BF in the mortar.

Table 7 shows the standards formulas of different countries for estimating the STS and FS based on the UCS. It is generally recognized that the relationship between the STS, FS and UCS of concrete can be expressed by using Equation (5). Based on the growth rate and previous standards in Table 7, $b = 0.75$ for STS and $b = 0.5$ for FS, respectively. The value of parameter a in Equation (5) is determined by fitting. Figure 18 displays the correlation between the STS and UCS of all mortar specimens. The correlation between the STS and UCS is significant, with $R^2 = 0.85$, which is also in good agreement with the results in Zheng [67] and Zheng [68].

$$f_{STS/FS} = a \times (f_{ucs})^b \quad (5)$$

3.4.3. Flexural Strength (FS)

The measured FS of single and hybrid fiber-reinforced specimens is illustrated in Figure 19. The specimens with fibers possess a larger FS than that of specimens in the control group without fibers. For single fiber-reinforced mortar, the FS displays an increasing trend with increasing fiber content. Overall, PANF causes greater improvements in FS than BF. In

addition, the improvement in FS of hybrid fibers is greater than that of single fibers. The maximum FS is 6.33 MPa for B0.25P0.05, which has increased by 15.65% compared with B0P0. In addition, the agglomeration of hybrid fibers leads to an increase in porosity and then decreases the FS, which is similar to the change in the UCS and STS. It should be noted that the FS of B0P0.05 is higher than that of B.25P0.01 and B0.05P0.01; therefore, PANF is better than BF in enhancing FS.



Figure 17. Typical failure modes of mortar specimens after split tensile tests.

Table 7. The standards formulas for estimating the STS and FS based on the UCS.

Standards	f_{STS}	Standards	f_{FS}
NZS 3101 [69]	$0.44 \times (f_{UCS})^{0.5}$	NZS 3101 [69]	$0.60 \times (f_{UCS})^{0.5}$
EC-04 [70]	$0.30 \times (f_{UCS})^{(2/3)}$	EC 04 [70]	$0.435 \times (f_{UCS})^{(2/3)}$
GB 50010 [71]	$0.19 \times (f_{UCS})^{0.75}$	DG/TJ [72]	$0.75 \times (f_{UCS})^{0.5}$
JSCE [73]	$0.23 \times (f_{UCS})^{(2/3)}$	IS 456 [74]	$0.70 \times (f_{UCS})^{0.5}$
ACI 318-11 [75]	$0.56 \times (f_{UCS})^{0.5}$	ACI 318-11 [75]	$0.62 \times (f_{UCS})^{0.5}$

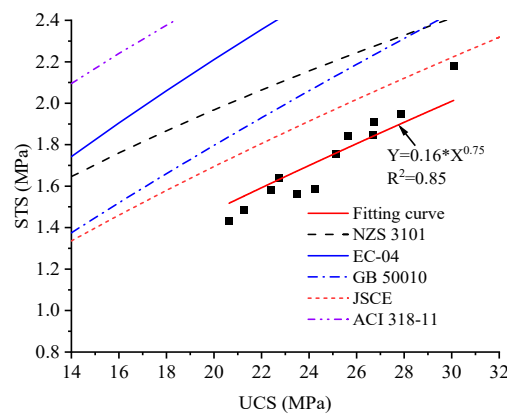


Figure 18. The relationship between the STS and UCS for the tailing mortar [69–71,73,75].

Figure 20 shows the failure modes of specimens after flexural tests. The B0P0 and B0P0.01 specimens exhibit brittle fracture characteristics. As the fiber content increases, the toughness of the specimen increases and the main cracks are narrow. For example, the main crack in B0.25P0.05 is almost invisible after failure and its FS is the largest.

Figure 21 displays the correlation between the FS and UCS for tailing specimens. Based on the slower growth rate of the experimental data, the best fit was chosen at $b = 0.5$. The correlation is significant, with $R^2 = 0.51$, which is consistent with previous findings in Zheng [67], Zheng [68] and Wang [26]. This implies that the change rule of all of the

strength indexes is similar for the fiber types and contents, and the best fiber combination is B0.25P0.05.

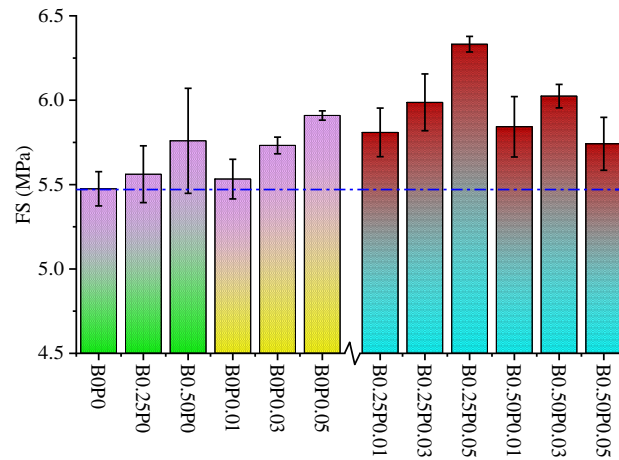


Figure 19. The FS against incorporated fiber content.

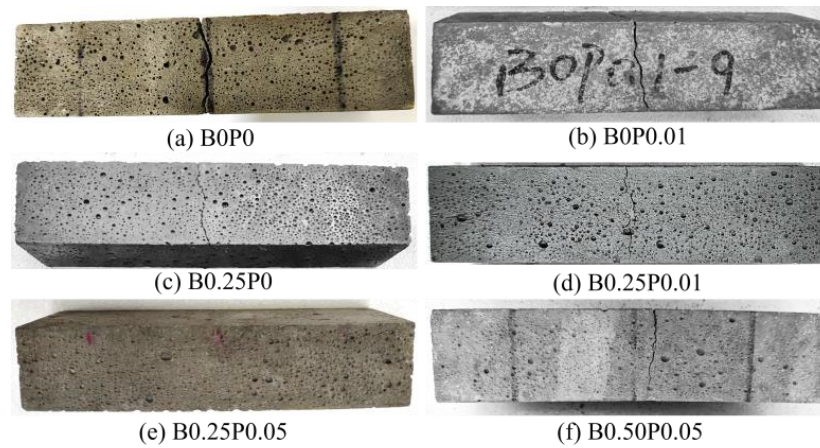


Figure 20. Typical failure mode of mortar specimens after flexural tests.

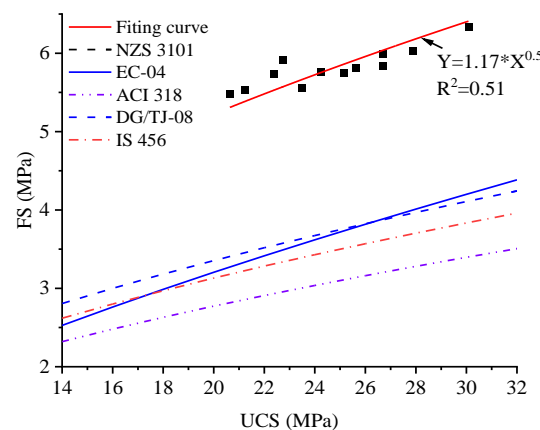


Figure 21. The relationship between the FS and UCS of mortar [69,70,72,74,75].

3.5. Quantification of the Synergy Effect of BF and PANF

Banthia [23] and Cui [76] proposed an index to evaluate the synergy effect of hybrid fibers in Equation (6). $M > 1$ represents a positive synergy effect, which means that the

improvement due to hybrid fibers is larger than the sum of all fibers added alone. When $M \leq 1$, the synergy effect is insignificant or negative.

$$M = \frac{f_{\text{hybrid},a+b} - f_0}{f_a + f_b - 2f_0} \quad (6)$$

where M is the synergy effect index; $f_{\text{hybrid},a+b}$ is the mechanical strength of the hybrid fiber-reinforced mortar; f_a and f_b are the mechanical strength of the single fiber-reinforced mortar; f_0 is the mechanical strength of the mortar without fibers.

Table 8 shows the synergetic effect index of the HRTM on mechanical strengths. It is evident that the combinations of fibers have played a positive role in the growth of strengths except for the B0.50P0.05 group, which is inconsistent with the change in the UCS, STS and FS. The synergistic effect of the B0.25P0.05 group is evident on the UCS and STS, both of which are optimal. However, the best synergistic effect on the FS occurs in the B0.25P0.01 group, because the flexural strength of B0P0.01 is much smaller than that of B0P0.05, and thus B0P0.01 has a much larger improvement potential due to the addition BFs. In addition, the synergistic effect of B0.25P0.05 is still much better than the other hybrid combinations in terms of FS.

Table 8. The synergetic effect of hybrid fibers.

Number	M		
	UCS	STS	FS
B0.25P0.01	1.444	2.215	2.321
B0.25P0.03	1.322	1.728	1.492
B0.25P0.05	1.918	2.224	1.646
B0.5P0.01	1.442	1.943	1.075
B0.5P0.03	1.356	1.703	1.014
B0.5P0.05	0.795	0.890	0.371

3.6. Economic Analysis of HRTM Specimens

In this study, 50% SS was used as aggregate for the preparation of the HRTM. However, when HRTM specimens are utilized on a large scale in actual construction, 50% natural sand is used as aggregate at a much lower cost than SS (in Wuhan, SS: 10.18 CNY/kg and natural sand: 0.156 CNY/kg). Therefore, the price of natural sand was calculated in the economic analysis of HRTM specimens. The prices of cement (42.5), natural sand and SP in Wuhan from July 2022 to June 2023 are calculated in Table 9. In addition, the prices of dry-mixed mortar are as follows: M20 is 0.372 CNY/kg and M25 is 0.418 CNY/kg. The price of tailings is preliminarily determined based on transportation distance. Furthermore, according to the proportions in this experiment, the prices of fiber-reinforced specimens can be further obtained in Table 10. Based on the mixing proportion of previous tests [12], the price of the mortar with only SS (B0P0-100% SS) is calculated in Table 9. Therefore, compared to the dry mortar, the HRTM used in this experiment has a good economic benefit. The prices of the HRTM (B0P0.01, B0.25P0.03 and B0.25P0.05) are more cost-effective and they have greater performance compared to B0.50P0. Further, the prices of the HRTM (B0P0.01, B0.25P0.03 and B0.25P0.05) are much lower than the price of B0P0-100% SS. Through economic analysis, it is also recommended to use the tailing mortar with 0.25% BF and 0.05% PANF.

Table 9. The prices of original materials in Wuhan (2022~2023). (Unit: CNY/kg).

Materials	Cement	Natural Sand	IOTs	SP	BF	PANF
Price	0.448	0.156	0.030	5.200	12.500	9.000

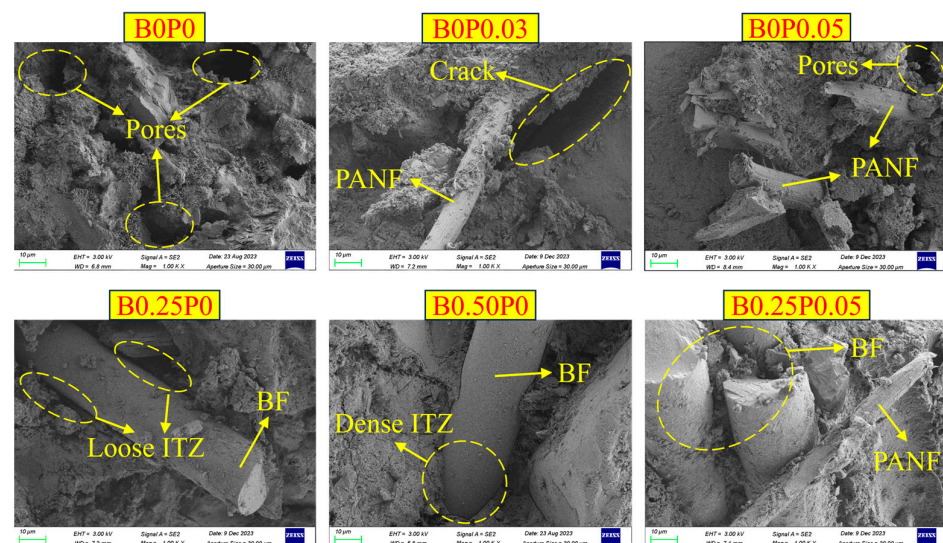
Table 10. The prices of hybrid fiber-reinforced mortar. (Unit: CNY/kg).

Number	Price
B0P0-100% SS	0.2127
B0P0	0.1701
B0.25P0	0.2013
B0.50P0	0.2326
B0P0.01	0.1710
B0P0.03	0.1728
B0P0.05	0.1746
B0.25P0.01	0.2022
B0.25P0.03	0.2040
B0.25P0.05	0.2058
B0.50P0.01	0.2335
B0.50P0.03	0.2353
B0.50P0.05	0.2371

3.7. Microstructure Analysis

3.7.1. SEM

The microstructure of the interface between the fibers and the matrix was further investigated by conducting SEM tests (Figure 22). It can be observed that there are many pores in the tailing mortar. With the addition of fibers, some pores and cracks inside the mortar are filled and bridged, leading to a dense structure. In the B0P0.03 and B0.25P0 groups, the bridging effect is weak when not many fibers are contained, and obvious pores and cracks occur. In addition, if the content of fibers is small, it is to pull them out or break them. In the B0P0.05 and B0.50P0 groups, due to the increase in fiber content, the bridging effect and the three-dimensional network structure are significant. Furthermore, in the B0.25P0.05 group, the three-dimensional network structure created by the hybrid BF and PANF is more obvious. Therefore, a suitable content of fibers provides enough cracking resistance to enhance the mechanical strengths [77]. With increasing fiber content, the interfacial bonding and interfacial transition zone (ITZ) between the fibers and the matrix are improved. BF and PANF with good hydrophilicity can absorb some water; therefore, the water/cement ratio near their surface is higher than the cement matrix and thus promotes early cement hydration [78]. In the B0.50P0.05 group, too many fibers are contained, which results in poor dispersion of hybrid fibers, as shown in Figure 23. The bonding effect between the fibers and the matrix decreases and the final strength also reduces.

**Figure 22.** Typical SEM micromorphology images of mortar specimens.

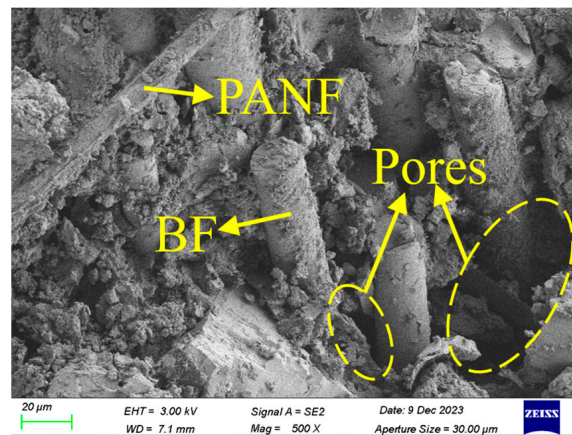


Figure 23. The agglomeration of excessive hybrid fibers.

3.7.2. XRD

Figure 24 displays the hydration product against the content of hybrid fibers. It can be observed that the main crystalline phases are SiO_2 , C-S-H, $\text{Ca}(\text{OH})_2$, CaSO_4 , AFt and CaCO_3 . The SiO_2 and CaCO_3 phases mainly exist in aggregates. C-S-H and $\text{Ca}(\text{OH})_2$ are produced by the hydration reactions of cement. The production of CaSO_4 and AFt can be explained as follows. The high sulfur content in fine IOTs is prone to separate out and further be oxidized to sulfur ions, which can react with $\text{Ca}(\text{OH})_2$ to form ettringite and gypsum. The addition of fibers does not change the type of hydration products, indicating that fibers are inert in the matrix. However, the amount of hydration products increases with the increasing content of hybrid fibers. Generally, the nucleation sites of the hydration products will increase after adding appropriate fibers, and thus promote the hydration reaction rate and produce more hydration products [30,79]. C-S-H and $\text{Ca}(\text{OH})_2$ are beneficial for the increase in strength, and CaSO_4 and AFt can also promote strength in the early stages. Therefore, a higher content of the four hydration products plays a positive and significant role in strength. Figure 24 shows that the B0.25P0.05 group possessed the highest amount of hydration products. Therefore, its mechanical strengths are the highest. Conversely, in B0.50P0.05, the agglomeration of hybrid fibers decreases the hydration rate, leading to a reduction in hydration products.

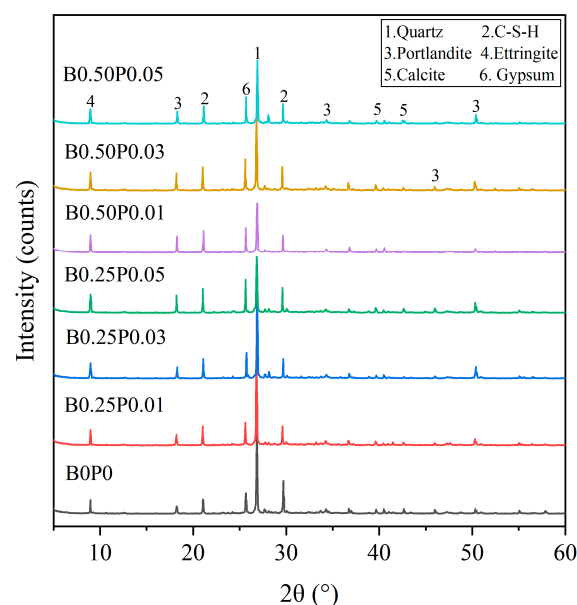


Figure 24. XRD patterns of mortar specimens.

4. Conclusions

This study investigated the physico-mechanical properties of tailing mortar reinforced with hybrid BF and PANF. In summary, the following conclusions can be drawn:

- (1) The addition of BF and PANF reduces the fluidity of tailing mortar; however, fibers significantly enhance the overall performance of the HRTM. Furthermore, hybrid fibers cause greater improvements in the physico-mechanical properties than single fibers. For example, the improvement due to hybrid fibers in porosity and ultrasonic wave velocity is much better than that due to a single fiber. The optimum hybrid fiber combination for the CS, STS and FS is B0.25P0.05. Compared to the tailing mortar without fibers, the CS, STS and FS increase by 45.74%, 52.33% and 15.65%, respectively. The enhancement effect of the STS is the largest.
- (2) The reinforced mechanism of the HRTM by adding fibers has been investigated. BF and PANF prevent the production and propagation of cracks and thus greatly improve the toughness of the mortar. BF (6 mm) has a better reinforcement effect that improves the UCS due to its high elastic modulus (63 GPa), while PANF (12 mm) is favorable to improve the STS and FS due to its better bridging effect and the creation of a denser network structure. However, when the fiber contents are excessive, the toughness decreases.
- (3) The synergetic effect of hybrid fibers on the tailing mortar have been evaluated, showing that all of the hybrid fiber combinations have a positive effect, except for B0.50P0.05. The B0.25P0.05 group possesses the largest synergetic effect index (UCS: 1.918; STS: 2.224), and the synergistic effect of B0.25P0.05 is still much better (FS: 1.646) than the other hybrid combinations in terms of FS. Moreover, it is also a very economical choice (0.2058 CNY/kg).
- (4) Observed through SEM tests, with increasing fiber content, the bond action between fibers and the matrix in the specimens is significant, which can improve the density of the tailing mortar. The XRD test shows that hybrid fibers cannot change the types of hydration products; however, they can provide more nucleation sites to promote the hydration reaction and improve the internal structure of the tailing mortar.

Therefore, it can be concluded that the most economical and high-performance combination of hybrid fibers for the HRTM is B0.25P0.05. In addition, it should also be noted that sulfur is harmful to the structure and long-term strength, and thus, the long-term performance of the HRTM should be investigated further.

Author Contributions: Conceptualization, J.X.; validation, Y.L., Z.C. and Y.S.; data curation, Y.L., Z.C. and Y.S.; writing—original draft preparation, Z.P. and S.H.; writing—review and editing, J.X., Z.P. and S.H.; visualization, Y.L., Z.C. and Y.S. All authors have read and agreed to the published version of the manuscript.

Funding: This work was supported by the National Natural Science Foundation of China (Grant No. 42377191 and 42072300) and the Project of the Natural Science Foundation of Hubei Province (Grand No. 2021CFA094). This work was supported by “The 14th Five Year Plan” Hubei Provincial advantaged characteristic disciplines (groups) project of Wuhan University of Science and Technology (Grant No. 2023A0303).

Data Availability Statement: Data will be made available upon request. The data are not publicly available due to privacy.

Conflicts of Interest: Author Jianbo Xu was employed by the company China First Metallurgical Group Co., Ltd. The remaining authors declare that the research was conducted in the absence of any commercial or financial relationships that could be construed as a potential conflict of interest.

References

1. Tiwari, A.; Singh, S.; Nagar, R. Feasibility Assessment for Partial Replacement of Fine Aggregate to Attain Cleaner Production Perspective in Concrete: A Review. *J. Clean. Prod.* **2016**, *135*, 490–507. [[CrossRef](#)]
2. Zhao, J.; Wang, Q.; Xu, G.; Shi, Y.; Su, Y. Influence of Macro-Synthetic Fiber on the Mechanical Properties of Iron Ore Tailing Concrete. *Constr. Build. Mater.* **2023**, *367*, 130293. [[CrossRef](#)]
3. Zhu, Q.; Yuan, Y.; Chen, J.; Fan, L.; Yang, H. Research on the High-Temperature Resistance of Recycled Aggregate Concrete with Iron tailing Sand. *Constr. Build. Mater.* **2022**, *327*, 126889. [[CrossRef](#)]
4. Zhang, N.; Tang, B.; Liu, X. Cementitious Activity of Iron Ore Tailing and Its Utilization in Cementitious Materials, Bricks and Concrete. *Constr. Build. Mater.* **2021**, *288*, 123022. [[CrossRef](#)]
5. Kefeni, K.K.; Msagati, T.A.M.; Mamba, B.B. Acid Mine Drainage: Prevention, Treatment Options, and Resource Recovery: A Review. *J. Clean. Prod.* **2017**, *151*, 475–493. [[CrossRef](#)]
6. Han, X.; Wang, Y.; Zhang, N.; Meng, J.; Li, Y.; Liang, J. Facile Synthesis of Mesoporous Silica Derived from Iron Ore Tailings for Efficient Adsorption of Methylene Blue. *Colloids Surf. B* **2021**, *617*, 126391. [[CrossRef](#)]
7. Shettima, A.U.; Hussin, M.W.; Ahmad, Y.; Mirza, J. Evaluation of Iron Ore Tailings as Replacement for Fine Aggregate in Concrete. *Constr. Build. Mater.* **2016**, *120*, 72–79. [[CrossRef](#)]
8. Zhou, Y.; Yang, Z.; You, Z.; Wang, X.; Chen, K.; Guo, B.; Wu, K. Experimental Study on Fire Resistance of Concrete Beams Made with Iron Tailings Sand. *Buildings* **2022**, *12*, 1816. [[CrossRef](#)]
9. Andrews, A.; Nyarko, E.F.; Adjaottor, A.A.; Nsiah-Baafi, E.; Adom-Asamoah, M. Reuse and Stabilization of Sulphide Mine Tailings as Fine Aggregate for Construction Mortar. *J. Clean. Prod.* **2022**, *357*, 131971. [[CrossRef](#)]
10. Zhang, W.; Gu, X.; Qiu, J.; Liu, J.; Zhao, Y.; Li, X. Effects of Iron Ore Tailings on the Compressive Strength and Permeability of Ultra-High Performance Concrete. *Constr. Build. Mater.* **2020**, *260*, 119917. [[CrossRef](#)]
11. Zhao, S.; Fan, J.; Sun, W. Utilization of Iron Ore Tailings as Fine Aggregate in Ultra-High Performance Concrete. *Constr. Build. Mater.* **2014**, *50*, 540–548. [[CrossRef](#)]
12. Huang, S.; Pi, Z.; Cai, C.; Li, H. Utilization of High-Sulfur Iron Ore Tailings in Cement Mortar by Considering the Influence of Curing Temperature and Tailing Content. *J. Build. Eng.* **2023**, *74*, 106826. [[CrossRef](#)]
13. Li, T.; Wang, S.; Xu, F.; Meng, X.; Li, B.; Zhan, M. Study of the Basic Mechanical Properties and Degradation Mechanism of Recycled Concrete with Tailings before and after Carbonation. *J. Clean. Prod.* **2020**, *259*, 120923. [[CrossRef](#)]
14. Xu, F.; Wang, S.; Li, T.; Liu, B.; Zhao, N.; Liu, K. The Mechanical Properties and Resistance against the Coupled Deterioration of Sulfate Attack and Freeze-Thaw Cycles of Tailing Recycled Aggregate Concrete. *Constr. Build. Mater.* **2021**, *269*, 121273. [[CrossRef](#)]
15. Xu, F.; Wang, S.; Li, T.; Liu, B.; Zhou, Y. Mechanical Properties and Pore Structure of Recycled Aggregate Concrete Made with Iron Ore Tailings and Polypropylene fibers. *J. Build. Eng.* **2021**, *33*, 101572. [[CrossRef](#)]
16. Adesina, A. Performance of Cementitious Composites Reinforced with Chopped Basalt Fibres—An Overview. *Constr. Build. Mater.* **2021**, *266*, 120970. [[CrossRef](#)]
17. Quan, X.; Wang, S.; Liu, K.; Xu, J.; Zhang, K.; Zhao, N.; Li, B. Influence of Iron Ore Tailings By-Product on the Mechanical and Electrical Properties of Carbon Fiber Reinforced Cement-Based Composites. *J. Build. Eng.* **2022**, *45*, 103567. [[CrossRef](#)]
18. Zhao, K.; Lai, Y.; He, Z.; Liu, W.; Zhao, R.; Wang, Y.; Tian, X.; Nie, J. Study on Energy Dissipation and Acoustic Emission Characteristics of Fiber Tailings Cemented Backfill with Different Ash-Sand Ratios. *Process Saf. Environ. Prot.* **2023**, *174*, 983–996. [[CrossRef](#)]
19. High, C.; Seliem, H.M.; El-Safty, A.; Rizkalla, S.H. Use of Basalt Fibers for Concrete Structures. *Constr. Build. Mater.* **2015**, *96*, 37–46. [[CrossRef](#)]
20. Zhang, C.; Wang, Y.; Zhang, X.; Ding, Y.; Xu, P. Mechanical Properties and Microstructure of Basalt Fiber-Reinforced Recycled Concrete. *J. Clean. Prod.* **2021**, *278*, 123252. [[CrossRef](#)]
21. Chinchillas-Chinchillas, M.J.; Orozco-Carmona, V.M.; Gaxiola, A.; Alvarado-Beltrán, C.G.; Pellegrini-Cervantes, M.J.; Baldenebro-López, F.J.; Castro-Beltrán, A. Evaluation of the Mechanical Properties, Durability and Drying Shrinkage of the Mortar Reinforced with Polyacrylonitrile Microfibers. *Constr. Build. Mater.* **2019**, *210*, 32–39. [[CrossRef](#)]
22. Pakravan, H.R.; Latifi, M.; Jamshidi, M. Hybrid Short Fiber Reinforcement System in Concrete: A Review. *Constr. Build. Mater.* **2017**, *142*, 280–294. [[CrossRef](#)]
23. Banthia, N.; Majdzadeh, F.; Wu, J.; Bindiganavile, V. Fiber Synergy in Hybrid Fiber Reinforced Concrete (HyFRC) in Flexure and Direct Shear. *Cem. Concr. Compos.* **2014**, *48*, 91–97. [[CrossRef](#)]
24. Hay, R.; Ostertag, C.P. Influence of Transverse Cracks and Interfacial Damage on Corrosion of Steel in Concrete with and without Fiber Hybridization. *Corros. Sci.* **2019**, *153*, 213–224. [[CrossRef](#)]
25. Walton, P.L.; Majumdar, A.J. Cement-Based Composites with Mixtures of Different Types of Fibres. *Compos. Commun.* **1975**, *6*, 209–216. [[CrossRef](#)]
26. Wang, D.; Ju, Y.; Shen, H.; Xu, L. Mechanical Properties of High Performance Concrete Reinforced with Basalt Fiber and Polypropylene Fiber. *Constr. Build. Mater.* **2019**, *197*, 464–473. [[CrossRef](#)]
27. de Sá, F.R.G.; Silva, F.d.A.; Cardoso, D.C.T. Tensile and Flexural Performance of Concrete Members Reinforced with Polypropylene Fibers and GFRP Bars. *Compos. Struct.* **2020**, *253*, 112784. [[CrossRef](#)]
28. Branston, J.; Das, S.; Kenno, S.Y.; Taylor, C. Mechanical Behaviour of Basalt Fibre Reinforced Concrete. *Constr. Build. Mater.* **2016**, *124*, 878–886. [[CrossRef](#)]

29. Kizilkanat, A.B.; Kabay, N.; Akyüncü, V.; Chowdhury, S.; Akça, A.H. Mechanical Properties and Fracture Behavior of Basalt and Glass Fiber Reinforced Concrete: An Experimental Study. *Constr. Build. Mater.* **2015**, *100*, 218–224. [[CrossRef](#)]
30. Fiore, V.; Scalici, T.; Di Bella, G.; Valenza, A. A Review on Basalt Fibre and Its Composites. *Compos. B. Eng.* **2015**, *74*, 74–94. [[CrossRef](#)]
31. Wang, Y.; Kang, A.-H.; Wu, Z.-G.; Xiao, P.; Gong, Y.-F.; Sun, H.-F. Investigation of the Basalt Fiber Type and Content on Performances of Cement Mortar and Concrete. *Constr. Build. Mater.* **2023**, *408*, 133720. [[CrossRef](#)]
32. Zeng, Y.; Li, X.; Tang, A.; Zhao, N.; Li, L.; Jia, S. Axial Compressive Behavior of Basalt and Polyacrylonitrile Fibers Reinforced Lightweight Aggregate Concrete with Industrial Waste Ceramsite-Lytag after Freeze-Thaw Cycles. *J. Build. Eng.* **2023**, *76*, 107402. [[CrossRef](#)]
33. Li, Z.; Dong, J.; Chen, H.; Wu, Z.; Feng, K.; Zhang, G.; Cheng, S.; Jiang, T. Mechanical Behaviour and Acoustic Emission Characteristics of Basalt Fibre Mortar Rubble under Uniaxial Cyclic Compression. *Constr. Build. Mater.* **2023**, *393*, 132145. [[CrossRef](#)]
34. Guler, S.; Akbulut, Z.F. Workability, Physical & Mechanical Properties of the Cement Mortars Strengthened with Metakaolin and Steel/Basalt Fibers Exposed to Freezing-Thawing Periods. *Constr. Build. Mater.* **2023**, *394*, 132100.
35. Zeng, Y.; Tang, A. Comparison of Effects of Basalt and Polyacrylonitrile Fibers on Toughness Behaviors of Lightweight Aggregate Concrete. *Constr. Build. Mater.* **2021**, *282*, 122572. [[CrossRef](#)]
36. Liu, J.; Xiao, S.; Shen, Z.; Xu, L.; Zhang, L.; Peng, J. Study on the Oxidative Stabilization of Polyacrylonitrile Fibers by Microwave Heating. *Polym. Degrad. Stab.* **2018**, *150*, 86–91. [[CrossRef](#)]
37. Fan, S. Mechanical and Durability Performance of Polyacrylonitrile Fiber Reinforced Concrete. *Mater. Res.* **2015**, *18*, 1298–1303. [[CrossRef](#)]
38. Zheng, D.; Song, W.; Fu, J.; Xue, G.; Li, J.; Cao, S. Research on Mechanical Characteristics, Fractal Dimension and Internal Structure of Fiber Reinforced Concrete under Uniaxial Compression. *Constr. Build. Mater.* **2020**, *258*, 120351. [[CrossRef](#)]
39. Zeng, Z.; Li, C.; Chen, Z.; Ke, L. Study on Mechanical Properties and Optimum Fiber Content for Basalt/Polyacrylonitrile Hybrid Fiber Reinforced Concrete. *Adv. Mater. Sci. Eng.* **2022**, *2022*, 11. [[CrossRef](#)]
40. GB 175-2007; Standardization Administration of the People's Republic of China, Common Portland Cement. Standards Press of China: Beijing, China, 2007.
41. GB/T 17671-2021; Standardization Administration of the People's Republic of China, Test Method of Cement Mortar Strength (ISO Method). Standards Press of China: Beijing, China, 2021.
42. GB/T 14684-2022; Standardization Administration of the People's Republic of China, Sand for Construction. Standards Press of China: Beijing, China, 2022.
43. JTG 3420-2020; Ministry of Transport of the People's Republic of China, Testing Methods of Cement and Concrete for Highway Engineering. China Communication Press: Beijing, China, 2020.
44. ASTM C597-09 (2009); American Society for Testing and Materials, Standard Test Method for Ultrasonic Pulse Velocity through Concrete. ASTM International: West Conshohocken, PA, USA, 2009.
45. Menta, P.K. Stability of Ettringite on Heating. *J. Am. Ceram. Soc.* **1972**, *55*, 55–57.
46. Shahjalal, M.; Islam, K.; Rahman, J.; Ahmed, K.S.; Karim, M.R.; Billah, A.M. Flexural Response of Fiber Reinforced Concrete Beams with Waste Tires Rubber and Recycled Aggregate. *J. Clean. Prod.* **2021**, *278*, 123842. [[CrossRef](#)]
47. Yang, L.; Jia, H.; Wu, A.; Jiao, H.; Chen, X.; Kou, Y.; Dong, M. Particle Aggregation and Breakage Kinetics in Cemented Paste Backfill. *Int. J. Miner. Metall. Mater.* **2023**, *accepted*. [[CrossRef](#)]
48. Yang, L.; Jia, H.; Jiao, H.; Dong, M.; Yang, T. The Mechanism of Viscosity-Enhancing Admixture in Backfill Slurry and the Evolution of Its Rheological Properties. *Minerals* **2023**, *13*, 1045. [[CrossRef](#)]
49. Li, L.G.; Ouyang, Y.; Ng, P.-L.; Zeng, K.; Kwan, A.K.H. Influences of Fiber Length and Water Film Thickness on Fresh Properties of Basalt Fiber-Reinforced Mortar. *J. Zhejiang Univ.-Sci. A* **2021**, *22*, 344–356. [[CrossRef](#)]
50. Hossain, F.M.Z.; Pal, A.; Ahmed, K.S.; Bediwy, A.; Alam, M.S. Shear Behavior of Polypropylene Fiber-Reinforced Concrete Beams Containing Recycled Aggregate and Crumb Rubber. *J. Clean. Prod.* **2023**, *412*, 137370. [[CrossRef](#)]
51. Saloni, A.; Parveen, J.; Pham, T.M. Enhanced Properties of High-Silica Rice Husk Ash-Based Geopolymer Paste by Incorporating Basalt Fibers. *Constr. Build. Mater.* **2020**, *245*, 118422. [[CrossRef](#)]
52. Li, L.G.; Zhuo, H.X.; Zhu, J.; Kwan, A.K.H. Packing Density of Mortar Containing Polypropylene, Carbon or Basalt Fibres under Dry and Wet Conditions. *Powder Technol.* **2019**, *342*, 433–440. [[CrossRef](#)]
53. Li, L.; Zhao, Z.; Zhu, J.; Kwan, A.K.H.; Zeng, K. Combined Effects of Water Film Thickness and Polypropylene Fibre Length on Fresh Properties of Mortar. *Constr. Build. Mater.* **2018**, *174*, 586–593. [[CrossRef](#)]
54. Hwang, J.P.; Kim, M.; Ann, K.Y. Porosity Generation Arising from Steel Fibre in Concrete. *Constr. Build. Mater.* **2015**, *94*, 433–436. [[CrossRef](#)]
55. Zhang, Y.; Zheng, Y.; Du, C.; Hu, S.; Wang, Z. Hybrid Effects of Basalt and Polyvinyl Alcohol Fibers on the Mechanical Properties and Macro-Microscopic Analysis of Low-Heat Portland Cement Concrete. *J. Mater. Res. Technol.* **2023**, *25*, 608–632. [[CrossRef](#)]
56. Benaicha, M.; Jalbaud, O.; Hafidi Alaoui, A.; Burtschell, Y. Correlation between the Mechanical Behavior and the Ultrasonic Velocity of Fiber-Reinforced Concrete. *Constr. Build. Mater.* **2015**, *101*, 702–709. [[CrossRef](#)]
57. Ridengaoqier, E.; Hatanaka, S.; Palamy, P.; Kurita, S. Experimental Study on the Porosity Evaluation of Pervious Concrete by Using Ultrasonic Wave Testing on Surfaces. *Constr. Build. Mater.* **2021**, *300*, 123959.

58. Zhang, P.; Wang, K.; Wang, J.; Guo, J.; Ling, Y. Macroscopic and Microscopic Analyses on Mechanical Performance of Metakaolin/Fly Ash Based Geopolymer Mortar. *J. Clean. Prod.* **2021**, *294*, 126193. [[CrossRef](#)]
59. Miah, M.J.; Li, Y.; Paul, S.C.; Babafemi, A.J.; Jang, J.G. Mechanical Strength, Shrinkage, and Porosity of Mortar Reinforced with Areca Nut Husk Fibers. *Constr. Build. Mater.* **2023**, *363*, 129688. [[CrossRef](#)]
60. Li, K.F.; Yang, C.Q.; Huang, W.; Zhao, Y.B.; Wang, Y.; Pan, Y.; Xu, F. Effects of Hybrid Fibers on Workability, Mechanical, and Time-Dependent Properties of High Strength Fiber-Reinforced Self-Consolidating Concrete. *Constr. Build. Mater.* **2021**, *277*, 122325. [[CrossRef](#)]
61. Das, C.S.; Dey, T.; Dandapat, R.; Mukharjee, B.B.; Kumar, J. Performance Evaluation of Polypropylene Fibre Reinforced Recycled Aggregate Concrete. *Constr. Build. Mater.* **2018**, *189*, 649–659. [[CrossRef](#)]
62. Niu, D.; Su, L.; Luo, Y.; Huang, D.; Luo, D. Experimental Study on Mechanical Properties and Durability of Basalt Fiber Reinforced Coral Aggregate Concrete. *Constr. Build. Mater.* **2020**, *237*, 117628. [[CrossRef](#)]
63. Duan, M.; Qin, Y.; Li, Y.; Wei, Y.; Geng, K.; Zhou, H.; Liu, R. Mechanical Properties and Multi-Layer Perceptron Neural Networks of Polyacrylonitrile Fiber Reinforced Concrete Cured Outdoors. *Structures* **2023**, *56*, 104954. [[CrossRef](#)]
64. Sadrinejad, I.; Madandoust, R.; Ranjbar, M.M. The Mechanical and Durability Properties of Concrete Containing Hybrid Synthetic Fibers. *Constr. Build. Mater.* **2018**, *178*, 72–82. [[CrossRef](#)]
65. Teng, S.; Afroughsabet, V.; Ostertag, C.P. Flexural Behavior and Durability Properties of High Performance Hybrid-Fiber-Reinforced Concrete. *Constr. Build. Mater.* **2018**, *182*, 504–515. [[CrossRef](#)]
66. Nazir, K.; Canpolat, O.; Uysal, M.; Niş, A.; Kuranlı, Ö.F. Engineering Properties of Different Fiber-Reinforced Metakaolin-Red Mud Based Geopolymer Mortars. *Constr. Build. Mater.* **2023**, *385*, 131496. [[CrossRef](#)]
67. Zheng, W.; Wang, S.; Quan, X.; Qu, Y.; Mo, Z.; Lin, C. Carbonation Resistance and Pore Structure of Mixed-Fiber-Reinforced Concrete Containing Fine Aggregates of Iron Ore Tailings. *Materials* **2022**, *15*, 8992. [[CrossRef](#)]
68. Zheng, Y.; Zhuo, J.; Zhang, P.; Ma, M. Mechanical Properties and Meso-Microscopic Mechanism of Basalt Fiber-Reinforced Recycled Aggregate Concrete. *J. Clean. Prod.* **2022**, *370*, 133555. [[CrossRef](#)]
69. NZS 3101; Concrete Structures Standard: Part 1: The Design of Concrete Structures. Standards New Zealand: Wellington, New Zealand, 2006.
70. EC-04. B.S.; Eurocode 2: Design of Concrete Structures: Part 1-1: General Rules and Rules for Buildings. European Committee for Standardization: Brussels, Belgium, 2004.
71. GB 50010-2010; Chinese Standard: Code for Design of Concrete Structures. China Building Press: Beijing, China, 2010.
72. DG/TJ-08; Technical Code for Application of Recycled Aggregate Concrete. Shanghai Construction Standard Society (SCSS): Shanghai, China, 2017.
73. JSCE, 2007; Standard Specification for Concrete Structure. Japan Society of Civil Engineers: Tokyo, Japan, 2007.
74. IS 456; Plain and Reinforced Concrete Code of Practice. Bureau of Indian Standards Indian Standard: New Delhi, India, 2000.
75. ACI 318-11; Concrete Institute & International Organization for Standardization, Building Code Requirements for Structural Concrete and Commentary. American Concrete Institute: Farmington Hills, MI, USA, 2011.
76. Cui, K.; Xu, L.; Tao, T.; Huang, L.; Li, J.; Hong, J.; Li, H.; Chi, Y. Mechanical Behavior of Multiscale Hybrid Fiber Reinforced Recycled Aggregate Concrete Subject to Uniaxial Compression. *J. Build. Eng.* **2023**, *71*, 106504. [[CrossRef](#)]
77. Hong, L.; Chen, Y.D.; Li, T.D.; Gao, P.; Sun, L.Z. Microstructure and Bonding Behavior of Fiber-Mortar Interface in Fiber-Reinforced Concrete. *Constr. Build. Mater.* **2020**, *232*, 117235. [[CrossRef](#)]
78. Liang, N.; Geng, S.; Mao, J.; Liu, X.; Zhou, X. Investigation on Cracking Resistance Mechanism of Basalt-Polypropylene Fiber Reinforced Concrete Based on SEM Test. *Constr. Build. Mater.* **2024**, *411*, 134102. [[CrossRef](#)]
79. Chen, X.; Shi, X.; Zhou, J.; Chen, Q.; Li, E.; Du, X. Compressive Behavior and Microstructural Properties of Tailings Polypropylene Fibre-Reinforced Cemented Paste Backfill. *Constr. Build. Mater.* **2018**, *190*, 211–221. [[CrossRef](#)]

Disclaimer/Publisher's Note: The statements, opinions and data contained in all publications are solely those of the individual author(s) and contributor(s) and not of MDPI and/or the editor(s). MDPI and/or the editor(s) disclaim responsibility for any injury to people or property resulting from any ideas, methods, instructions or products referred to in the content.